Journal of Nanobiotechnology

RESEARCH

Open Access

# *Momordica charantia* L.-derived exosome-like nanovesicles stabilize p62 expression to ameliorate doxorubicin cardiotoxicity

Cong Ye[1†], Chen Yan[2†], Si-Jia Bian[1], Xin-Ran Li[1], Yu Li[3], Kai-Xuan Wang[4], Yu-Hua Zhu[1], Liang Wang[1], Ying-Chao Wang[1], Yi-Yuan Wang[1], Tao-Sheng Li[5], Su-Hua Qi[1*] and Lan Luo[1*]

## Abstract

**Background** Doxorubicin (DOX) is a first-line chemotherapeutic drug for various malignancies that causes cardiotoxicity. Plant-derived exosome-like nanovesicles (P-ELNs) are growing as novel therapeutic agents. Here, we investigated the protective effects in DOX cardiotoxicity of ELNs from *Momordica charantia* L. (MC-ELNs), a medicinal plant with antioxidant activity.

**Results** We isolated MC-ELNs using ultracentrifugation and characterized them with canonical mammalian extracellular vesicles features. In vivo studies proved that MC-ELNs ameliorated DOX cardiotoxicity with enhanced cardiac function and myocardial structure. In vitro assays revealed that MC-ELNs promoted cell survival, diminished reactive oxygen species, and protected mitochondrial integrity in DOX-treated H9c2 cells. We found that DOX treatment decreased the protein level of p62 through ubiquitin-dependent degradation pathway in H9c2 and NRVM cells. However, MC-ELNs suppressed DOX-induced p62 ubiquitination degradation, and the recovered p62 bound with Keap1 promoting Nrf2 nuclear translocation and the expressions of downstream gene HO-1. Furthermore, both the knockdown of Nrf2 and the inhibition of p62-Keap1 interaction abrogated the cardioprotective effect of MC-ELNs.

**Conclusions** Our findings demonstrated the therapeutic beneficials of MC-ELNs via increasing p62 protein stability, shedding light on preventive approaches for DOX cardiotoxicity.

**Keywords** *Momordica charantia* L.-derived exosome-like nanovesicles, Doxorubicin cardiotoxicity, p62/Keap1, Ubiquitination, Nrf2

†Cong Ye and Chen Yan contributed equally to this work.

*Correspondence:
Su-Hua Qi
suhuaqi@xzhmu.edu.cn
Lan Luo
luolan@xzhmu.edu.cn
[1]School of Medical Technology, Xuzhou Key Laboratory of Laboratory Diagnostics, Xuzhou Medical University, Xuzhou city, Jiangsu Province 221004, PR China
[2]Department of Rheumatology, The Second Affiliated Hospital, Jiangxi Medical College, Nanchang University, Nanchang city, Jiangxi Province, PR China
[3]Department of Anesthesiology, The Second Affiliated Hospital, Jiangxi Medical College, Nanchang University, Nanchang city, Jiangxi Province, PR China
[4]Department of Laboratory Medicine, Affiliated Hospital of Xuzhou Medical University, Xuzhou city, Jiangsu Province, PR China
[5]Department of Stem Cell Biology, Atomic Bomb Disease Institute, Nagasaki University, 1-12-4 Sakamoto, Nagasaki 852-8523, Japan

## Background

Doxorubicin (DOX) is a widely prescribed anti-cancer drug for a broad spectrum of cancers, including hematopoietic malignancies (leukemia, lymphoma) and solid tumors (ovary, breast, prostate, and gastrointestinal). Despite the outstanding curative effects of DOX, its propensity for inducing dose-dependent cardiotoxicity hampers its clinical practice. Acute DOX cardiotoxicity featured by reduced left ventricular ejection fraction (LVEF) is often apparent and manifests days after a single dose or course of therapy. Whereas long-term cardiotoxicity is difficult to predict and irreversible, which develops into cardiomyopathy and ultimately heart failure [1]. Though clinical features of DOX cardiotoxicity are well-documented, the exact mechanisms remain unclear, appearing complex and multifactorial. The proposed mechanisms comprise oxidative stress, topoisomerase II β inhibition, mitochondrial dysfunction, impaired autophagy, and alterations of cell death pathways such as apoptosis, necroptosis, ferroptosis, and pyroptosis [2]. After decades of basic research, dexrazoxane is still the only FDA-approved agent for preventing DOX cardiotoxicity, but its clinical use is limited due to decreased tumor response rate to DOX and risks of second malignancies [3]. In addition, the protective action of other cardiovascular drugs like angiotensin inhibitors and β-blockers against DOX cardiotoxicity lacks compelling clinical evidence [4]. Considering the widespread use of DOX, alternative management strategies are promptly required.

Extracellular vesicles (EVs) are lipid bilayer nano-sized particles secreted from mammalian cells and can regulate physiological processes via intercellular communication through their biological cargos, including proteins, nucleic acids, and metabolites. During the last two decades, EVs have propelled tremendous interest because of their potential to treat various diseased states and encapsulate therapeutic molecules, which offer a novel approach in treating cardiovascular disease and other diseases [5]. Recently, it identified that plant cells also release exosome-like nanovesicles (P-ELNs), biogenically, and morphologically identical to mammalian EVs. As the source of P-ELNs is edible plants, they are non-toxicity, biocompatible, biodegradable without inducing immunogenicity and carrying pathogens, and are high-yield with large-scalability production, enabling wide investigations as platforms for drug delivery [6, 7]. Moreover, P-ELNs transport bioactive components and could be internalized by mammalian cells displaying various therapeutic activities. P-ELNs from ginger, lemon, grapefruits, grape, and broccoli could be used for treating colitis. Others reported the anti-cancer actions of P-ELNs from lemon (chronic myeloid leukemia), *Asparagus cochinchinensis* (hepatocellular carcinoma), ginseng (melanoma), and ginger (colorectal cancer). In addition, P-ELNs showed therapeutic benefits in treating liver disease (ginger, garlic, honey, mushrooms), periodontitis (ginger), dermatitis (*Dendropanax morbifera*), and osteoporosis (yam) [6–8]. Overall, P-ELNs are emerging as a novel therapeutic class alternative to mammalian-derived EVs.

*Momordica charantia* L. (MC), or bitter melon, widely bred as a type of Cucurbitaceae vegetable, is a traditional medicinal plant. Several studies have reported that MC extracts show various medicinal properties such as antidiabetic, anti-cancer, anti-inflammatory, antioxidant, immune-modulatory, and neuro/hepato-protective function [9]. Chen et al. showed that P-ELNs from bitter melon promote the therapeutic efficacy of 5-fluorouracil on oral squamous cell carcinoma [10]. We demonstrated that P-ELNs derived from MC (MC-ELNs) inhibited glioma cell proliferation [11], exerted neuroprotective effects against ischemic brain injury [12], and prevented cardiomyocytes from ionizing radiation injury [13]. In the current study, we aimed to investigate the therapeutic role of MC-ELNs in mitigating DOX cardiotoxicity. Employing pharmacological and biological approaches, we proved the cardioprotective effect of MC-ELNs against DOX in vivo and in vitro. At the mechanism level, we observed that DOX-induced ubiquitination degradation of p62 was restored by MC-ELNs, promoting cardiomyocyte survival. Collectively, these findings provide proof of concept that MC-ELNs or interventions stabilizing p62 protein level are novel therapeutic avenues for mitigating cardiotoxicity in cancer patients receiving DOX therapy.

## Methods

### Isolation of *Momordica charantia* L.-derived exosome-like nanovesicles (MC-ELNs)

MC-ELNs were isolated from the fresh MC juice (Mengyang, Xishuangbanna, Yunnan Province, China.) as described in our previous study with modification [13]. In brief, MC was gently washed twice with deionized water and then squeezed with the juice extractor. First, the MC juice underwent sequential centrifugation at 1 000 g for 10 min, 3 000 g for 20 min, and 10 000 g for 40 min at 4℃. Then, the supernatant was centrifuged at 150 000 g for 90 min at 4℃ (Optima XE-90, Beckman Coulter Life Sciences, Indianapolis, U.S.). After the first ultracentrifugation, the pellet was suspended in ice-cold phosphate-buffered saline (PBS) and went through with a 0.22 μm filter (SLGV004SL, Millipore). The remaining supernatant was re-centrifuged at 150 000 g for 90 min at 4℃. The acquired pellet was suspended in 500 μl of PBS and went through with a 0.22 μm filter. Final samples of MC-ELNs were aliquoted and stored at −80℃ for further experiments. The protein concentration of MC-ELNs was evaluated by the BCA assay kit (23235, Thermo Fisher Scientific).

#### Biological electron microscopy

For Bio-EM analyses, samples were applied to FORMVAR FILM (BZ16226b, Beijing Zhongjingkeyi Technology Co., Ltd) dyed for 3 ~ 5 min and stained with 3% phosphotungstic acid. The film was observed and analyzed using biological electron microscopy (Tecnai G2 Spirit Twin, FEI, U.S.).

#### Nanoparticle tracking analysis

The size distribution of MC-ELNs were measured by nanoparticle tracking analysis (ZetaView, Particle Metrix, Germany). As the manual described, the MC-ELNs were diluted with PBS and then inserted to the analytical cell. The data of size distribution was acquired.

#### MC-ELNs RNA degradation

RNA degradation was performed by suspending MC-ELNs pellets in 0.2 mL of PBS as previously reported [14]. To one sample, 10 µl of Triton X100 (VIC398, VICMED) was added to achieve 5% Triton X100 concentration. MC-ELNs were incubated with 0.4 µg/mL RNase A (CW0601, CWBIO) treatment for 10 min at 37℃. Samples were further incubated with 0.1 mg/mL Proteinase K (ST533, Beyotime) for 20 min at 37℃. RNA was purified from samples using a miRNA isolation kit (RC201, Vazyme). RNA concentrations were determined using Nanodrop (840-317400, Thermo Fisher Scientific).

#### In vivo biodistribution of MC-ELNs

For the in vivo biodistribution of MC-ELNs, MC-ELNs were first labeled with DIR fluorescent dye (HY-D1048, MCE) by incubation at 37°C for 30 min according to the instructions. The solution was then ultracentrifuged at 150 000 g for 90 min at 4℃ and resuspended in 200 µl of ice-cold PBS to achieve DIR-MC-ELNs. C57BL/6J male mice were intravenously administrated with PBS, DIR or DIR-MC-ELNs (800 µg/kg), and then euthanized at 24 h. The liver, spleen, intestine, lung, brain, kidney, thymus, and heart tissues were harvested to track the distribution of MC-ELNs by ex vivo imaging analysis. DIR fluorescent signals were determined and quantified using the NEWTON7.0 FT100 (Vilber, France).

#### Proteomic, lipidomic, metabolomic analysis and bioinformatics analysis

MC-ELNs (600 µl) was stored at −80°C before proteomic, lipidomic and metabolomic analysis by Shanghai Biotree Medical Technology Company Ltd [15, 16]. Briefly, the protein was used for subsequent detection after acetone precipitation, re-solubilization, reduction, alkylation, enzymatic hydrolysis, removal of SDC and polypeptide desalting. The peptides were separated and analyzed with a nano-UPLC (EASY-nLC1200) coupled to a Q Exactive HFX Orbitrap instrument with a nano-electrospray ion source. Separation was performed using a reversed phase column (100 µm ID ×15 cm, Reprosil-Pur 120 C18AQ, 1.9 µm).

The MC-ELNs sample added with 160 µl iced methanol. Samples were de-proteined in water bath at 10°C for 30 min and then added with 800 µl methyl tert-butyl ether (MTBE). The supernatant was dried with nitrogen gas and reconstituted in isopropanol/methanol (50:50, v-v) for analysis. Instrumental analysis was performed by using ultra-high performance liquid chromatography (UHPLC) coupled with a timsTOF Pro2 instrument (Bruker). The mobile phase A is acetonitrile/water (60:40, containing 0.1% formic acid and 0.1% ammonium formate, v-v), and mobile phase B is isopropanol/acetonitrile (90:10, 0.1% formic acid, 0.1% ammonium formate, v-v).

An Untargeted metabolomic analysis based on a UHPLC-QE-MS system was used in this study. Samples containing at least ~ $10^{10}$ EVs particles determined by NTA were used for untargeted metabolite profiling by LC-MS. Each sample was mixed with 1000 µl extract solution (MeOH: ACN: H2O, 2:2:1 (v/v)). After vortex and sonication, we took out 250 µl supernatant and mixed it with resuspension buffer. The mobile phase A is water (containing 0.01% acetic acid), and mobile phase B is isopropanol/acetonitrile (50:50, v-v). We used an UHPLC system (Vanquish, Thermo Fisher Scientific) with a Phenomenex Kinetex C18 (2.1 mm × 50 mm, 2.6 µm) coupled to Orbitrap Exploris 120 mass spectrometer (Orbitrap MS, Thermo) for mass spectral analysis. The raw data were converted to the mzXML format using ProteoWizard and processed with an in-house program.

#### DOX cardiotoxicity animal model

Healthy 8 ~ 12 weeks C57BL/6J male mice (GemPharmatech Co., ltd) and Sprague Dawley male rats (Laboratory Animal Center, Xuzhou Medical University) weighed 220 ~ 250 g were used in this study. All mice and rats were housed with a 12-h light/12-h dark environmental cycle and at a controlled temperature. The animal protocols were approved by the Institutional Animal Care and Use Committee of Xuzhou Medical University (Approval no. 202210S017) and conducted strictly according to the Guiding Principles for the Use of Laboratory Animals.

The DOX cardiotoxicity model was established by a single intraperitoneally administration of DOX (#GC17567, GLPBIO) with a dose of 15 mg/kg to the mice or rats [17]. For the DOX cardiotoxicity mice model, animals were intravenously injected with a dose of 0, 800, and 1200 µg/kg of MC-ELNs once before and three times after the DOX administration, respectively. For the DOX cardiotoxicity rat model, animals were intravenously injected with a dose of 0 and 800 µg/kg of MC-ELNs once before and twice after the DOX administration, respectively.

Last, animals were sacrificed to collect blood samples and heart tissues. The blood sample was centrifuged at 3500 rpm for 10 ~ 15 min at 4°C to obtain the serum. Fresh heart tissue was fixed in 4% paraformaldehyde to prepare transverse paraffin section (4 μm). The paraffin heart sections were further processed for hematoxylin and eosin (H&E) staining and wheat germ agglutinin (WGA) staining (FL-1021-5, Vector). The H&E images were observed and scanned using a microscope inspection (Olympus VS120). The WGA images were observed under confocal microscopy (STELLARIS 5 Confocal Microscope, Leica Microsystems, Illinois, U.S.). The cardiomyocytes cross-sectional areas were analyzed using Image-J software (Fiji).

#### Determination of cardiac injury biomarkers

Serum cardiac injury biomarkers CK-MB (#E-EL-M0355c, Elabscience) and cTnT (#E-EL-M1801c, Elabscience) concentrations were measured by ELISA assay kits. The absorbance at 450 nm was measured using a microplate reader (Infinite F50, TECAN, Switzerland). The concentrations were calculated based on a standard curve equation.

#### Echocardiography

For the DOX cardiotoxicity rat model, cardiac function was evaluated under light anesthesia (2% isoflurane, R510-22-10, RWD) by the echocardiography (VINNO5×6–16 L, VINNO, Jiangsu, China). Parasternal short-axis M-mode image was obtained at the papillary level. The data of %Left ventricular (LV) fractional shortening (%LVFS) and %LV ejection fraction (%LVEF) were acquired. Other echocardiographic parameters such as the ventricular dimensions at end-systole (LVIDs), end-systolic volume (ESV), and stroke volume (SV) were measured.

#### Cell culture

The rat cardiomyocyte cell line (H9c2) and human breast cancer cell line (MCF-7) were purchased from the National Collection of Authenticated Cell Cultures (Shanghai, China). H9c2 and MCF-7 cells were cultured in Dulbecco's modified Eagle's High glucose (KGM12800N-500, KeyGEN BioTECH) supplemented with 10% fetal bovine serum (FBS, 10091-148, Gibco), 100 U/mL penicillin and 0.1 mg/mL streptomycin (15140122, Gibco). Cells were maintained in a humidified incubator (37℃, 5% $CO_2$, HeracellTM 150i, Thermo Fisher Scientific). Cells were treated with DOX (1 μM, GC17567, GLPBIO), Lactacystin (2 μM, Santa Cruz #sc-3575), Chloroquine (CQ, 5 μM for 24 h or 50 μM for 4 h, HY-17589 A, MCE), Rapamycin (100 nM, HY-10219, MCE), Cycloheximide (10 μg/mL, HY-12320, MCE), K67 inhibitor (100 μM, HY-111126, MCE).

#### Neonatal rat ventricular myocyte cells (NRVM) isolation

NRVM were isolated from the neonatal rat heart according to previous reports [18]. Briefly, the ventricular myocyte cells of neonatal rats were isolated quickly and transferred to the 0.1% trypsin solution. The trypsin solution was placed on a rocker in 4°C refrigerator overnight. Next day, the heart tissues were digested repeatedly with 1 mg/mL collagenase II (LS004176, Worthington) to harvest single cells. Non-myocyte was removed by differential adhesion method. The pure NRVM were cultured with IMDM (KGM12200N-500, KeyGEN BioTECH), 10% FBS, 100 U/mL penicillin and streptomycin, 200 μM L-glutamine (25030081, Gibco), 55 μM 2-mercaptoethanol (21985023, Gibco) and cultured in 5% $CO_2$ standard incubator at 37℃.

#### Cell viability assay

Cell viability was assessed by the Cell Proliferation Kit I (MTT assay, 11465007001, Roche Life Science). The H9c2 cells ($1\times10^4$ cells/well) and MCF-7 cells ($5\times10^3$ cells/well) were seeded in a 96-well culture plate. For the therapeutic effects of MC-ELNs in DOX cardiotoxicity, the H9c2 cells were pre-treated with 0, 0.5, 5, 10, 25 μg/mL of MC-ELNs for 6 h and then exposed to DOX (1 μM) for 24 h. For the safety evaluation of MC-ELNs, H9c2 and MCF-7 cells were treated with 0, 0.5, 5, 10, 25 μg/mL of MC-ELNs for 24h or 48 h. For the influence of MC-ELNs on DOX efficiency in MCF-7 cells, the MCF-7 cells were pre-treated with 0, 0.5, 5, 10, 25 μg/mL of MC-ELNs for 6 h and then exposed to DOX (1 μM) for 24 h. After indicated time of culture, 10 μl MTT labeling solution was added to each well and incubated at 37℃ for 4 h. Then, 100 μl solubilization solution was added to stop the formazan formation. Cells were cultured overnight and the absorbance at 562 nm was measured by an automatic microplate reader (Infinite F50, TECAN, Switzerland). The absorbance value of cells without treatment was included as a normalization control (%).

#### Lactate dehydrogenase (LDH) determination

The cytotoxicity of MC-ELNs on H9c2 cells were examined by the LDH Cytotoxicity Assay Kit (11644793001, Roche Life Science). H9c2 cells ($5\times10^3$ cells/well) were plated in a 96-well microplate, and MC-ELNs (0, 0.5, 5, 10, and 25 μg/mL) were added the next day. After 24 h of culture, the cell supernatant was transferred into a new microplate and incubated with reaction mixtures for 30 min, protected from light. The absorbance was detected at 490 nm and 680 nm by an automatic microplate reader (Synergy2, BioTEK, USA). The LDH activity in the culture media is directly proportional to the absorbance.

### Apoptosis assay

H9c2 cell apoptosis was assayed with the Annexin V-FITC/PI Apoptosis Detection Kit (556547, BD Biosciences) according to the manufacturer's instructions. The cells were harvested with 0.25% trypsin without EDTA (15090046, Gibco) and washed with PBS three times. Cells were resuspended in 100 μl of binding buffer. Then, 5 μl of Annexin V-FITC and 5 μl of PI were added to the cell suspensions at RT in the dark. After incubation for 15 min, the cells were added with 400 μl binding buffer. Cell apoptosis rate was analyzed using a flow cytometer within 1 h (FACS Canto II, Becton Dickinson, New Jersey, U.S.). The total cell apoptosis rate was the sum of Q3 and Q2 apoptosis rate.

### Western blot analysis and immunoprecipitation assay

After indicated treatments, H9c2 cells were homogenized with ice-cold RIPA buffer (89900, Thermo Scientific) containing 1% phosphatase and protease inhibitors (78442, Thermo Scientific). Total protein concentration was measured by BCA assay kit (23225, Thermo Scientific). The proteins were separated on SDS-PAGE gels (7.5%, 1610181, Bio-Rad; 10%, 1610183, Bio-Rad; 12%, 1610185, Bio-Rad) and transferred to 0.22 μm PVDF membranes (1620177, Bio-Rad) via Trans-Blot® Turbo™ transfer system (Bio-Rad, California, U.S.). Membranes were blocked with 5% skim milk in Tris Buffered Saline with Tween 20 (TBST) for 1 h at RT and then incubated with the primary antibody at 4°C overnight. The primary antibodies included Cleaved caspase3 (9664S, CST), Caspase3 (9665S, CST), Cleaved caspase7 (8438S, CST), Caspase7 (12827T, CST), Cleaved PARP (9545, CST), PARP (9532S, CST), γ-H2A.X (ab2893, Abcam), Cyclin D1 (2978S, CST), Cyclin E1 (20808S, CST), Cyclin B1 (4138S, CST), Nrf2 (SAB4501984, Sigma), HO-1 (10701-1AP, proteintech), SQSTM1/p62 (ab109012, Abcam), Keap1 (8047S, CST), Ubiquitin (ab140601, Abcam), K48-Ub (ab140601, Abcam), K63-Ub (ab179434, Abcam), TRIM21 (ab207728, Abcam), TRAF6 (HY-P80919, MCE), Parkin (ab77924, Abcam), PCNA (ab29, Abcam), LC3B (NB100-2220, NOVUS), NQO1 (67240-1-lg, proteintech), Catalase (21260-1-AP, proteintech), SOD2 (24127-1-AP, proteintech), GPX4 (ab125066, Abcam), β-actin (HRP-600008, proteintech). After sufficient washing with TBST, membranes were incubated with HRP-conjugated secondary antibodies for 1 h at RT. Blots were visualized using an ECL detection kit (KF8001, Affinity) using a ChemiDocTM Touch imaging system (Bio-Rad, California, U.S.). The density of the band was analyzed by the Image lab software (Bio-Rad, California, U.S.).

Co-IP analysis was performed as below. H9c2 cells were collected and lysed with cell lysis buffer (PR20037, proteintech) on ice. Lysates (500 μg) were incubated with 5 μl of anti-SQSTM1/p62 (ab109012, Abcam) at 4°C overnight. Then, 15 μl of Protein A/G Magnetic Beads (HY-K0202, MCE) was added and incubated for 2 h. The beads were washed with the same lysis buffer and subjected to western blotting as described above.

### Immunofluorescence staining

H9c2 cells were seeded on the chamber slide (177402PK, Thermo scientific). Cells were fixed with 4% paraformaldehyde for 10 min at RT. The cells were washed with PBS three times and blocked with 1% BSA with 0.1% Triton X100 at RT for 30 min. Then, cells were incubated with rat Ki-67 (14-5698-82, eBioscience), rabbit Nrf2 (SAB4501984, Sigma), mouse p62 (MA5-31498, Invitrogen), and rabbit Keap1 (8047S, CST) primary antibody at 4°C overnight, respectively. After washing with 0.05% PBST three times, cells were incubated with associated fluorescent secondary antibody anti-rabbit conjugated Alexa 488 (ab15077, Abcam), anti-rat conjugated Alexa 555 (ab150158, Abcam), anti-mouse conjugated Alexa 488 (ab150113, Abcam), anti-rabbit conjugated Alexa 546 (A-11035, Thermo scientific) for 60 min at RT. The cells were then washed with PBST three times and mounted in VECTASHIELD Antifade Mounting Medium with DAPI (H-1200, Vector).

H9c2 cells were seeded on the confocal dish (D35-20-0-N, Cellivs). Cell viability was evaluated by staining at 37°C for 30 min with calcein AM (1 μM) and ethidium homodimer-1 (4 μM) (L3224, Invitrogen) to visualize live (green) and dead (red) cells. Intracellular/mitochondrial ROS and mitochondrial morphology was visualized by labeling cells with 20 μM H2DCFDA (HY-D0940), 1 μM MitoSOX™ Red (M36008, Invitrogen), and 50 nM MitoTracker™ Green FM (M7514, Invitrogen) in the dark at 37°C for 30 min. The cells were stained with Hoechst 33342 (C1028, Beyotime) for 37°C for 10 min. Images were captured by confocal microscopy (STELLARIS 5 Confocal Microscope, Leica Microsystems, Illinois, U.S.).

### Mcherry-EGFP-LC3B reporter assay

mcherry-EGFP-LC3B reporter assay (GenePharma) were used to monitor the autophagy flux in H9c2 cells. Briefly, H9c2 cells ($1\times10^4$ cells) were prepared and infected at a multiplicity of infection (MOI) of 50 with lentiviruses and corresponding controls for 24 h at 37℃ in the presence of 4 μg/mL polybrene. Stably transfected cells were obtained through puromycin selection. The acidic environment of the lysosome quenches the green GFP fluorescence, whereas the red mCherry fluorescence is relatively stable. Therefore, yellow puncta ($GFP^+$/$mcherry^+$) stains the autophagosomes that have not fused with lysosomes, whereas the red puncta ($GFP^-$/$mcherry^+$) indicates the autolysosomes. Autophagy induction leads to an increase in both autophagosomes and autolysosomes. Inhibition of autophagy induction at

early stages leads to a decrease in both autophagosomes and autolysosomes. Inhibition of autophagy induction at late stages (e.g. inhibition of lysosomal acidification or lysosome fusion) leads to an increase in autophagosomes and a decrease in autolysosomes [19].

#### q-PCR analysis

Total RNA was isolated from cells using FastPure Cell/Tissue Total RNA Isolation Kit V2 (RC112, Vazyme), and 1 μg RNA was reverse-transcribed to cDNA with a PrimeScript™ RT reagent kit (RR037A, Takara). Then, qPCR was performed with ChamQ SYBR qPCR Master Mix (Q311-02, Vazyme) on a Roche LightCycler® 96 System (Hoffmann-La Roche Ltd, Switzerland). GAPDH was used as an internal control. Primers used in this study were listed as follows: p62, forward: 5′-CCAGCACAGG CACAGAAGATAAGAG-3′, reverse: 5′-TCCCACCGAC TCCAAGGCTATC-3′, GAPDH, forward: 5′- ACGGCA AGTTCAACGGCACAG-3′, reverse: 5′- CGACATACT CAGCACCAGCATCAC-3′.

#### siRNA transfection

H9c2 cells were plated overnight prior to transfection. Small interfering RNA of Nrf2 (50 nM, sc-156128, Santa Cruz) and scrambled siRNA (50 nM, sc-37007, Santa Cruz) were transfected into cells with Lipofectamine 3000 (L3000015, Invitrogen) according to manufacturer's instruction. After 48 h of incubation, cells were treated with or without MC-ELNs for the indicated time, and then harvested for western blot as described above.

#### Statistical analysis

All values are presented as the mean ± SD. The statistical significance between two groups was performed by two-tailed unpaired student's t-test. The statistical significance between three or more groups was performed by the ordinary one-way analysis of variance (ANOVA) followed by the Tukey's multiple comparisons test (assume all populations have the same SD) or Brown-Forsythe and Welch ANOVA tests followed by the Tamhane T2 multiple comparisons test (do not assume equal SDs) when data follow a normal distribution. Data between groups for non-normally distributed variables were compared by Kruskal–Wallis test followed by Dunn's test (GraphPad Prism 10.0.2). Differences were considered significant when $P < 0.05$.

## Results

#### Isolation and biological properties of MC-ELNs

The isolation protocol of MC-ELNs was outlined in Fig. 1A. In brief, fresh MC juice first underwent a sequential centrifugation (1 000 g, 10 min; 3 000 g, 20 min; 10 000 g, 40 min). Then, the supernatants underwent twice ultracentrifugation (150 000 g, 90 min). The pellet was suspended in PBS and passed through a 0.22 μm filter to obtain MC-ELNs. Biological electron microscopy (Bio-EM) and nanoparticle tracking analysis (NTA) revealed that MC-ELNs had an identical circular-shaped vesicular morphology (Fig. 1B) with an average diameter of 155 nm (Fig. 1C). By exposing the MC-ELNs to RNase A, proteinase K (added to dissociate protein complexes that may shield RNA), with or without 5% Triton X100 (added to permeabilize vesicles membrane), we confirmed that RNA enriched within the MC-ELNs (Fig. 1D). SDS-polyacrylamide gel electrophoresis identified the molecules sizes of proteins in MC-ELNs ranging from 10 to 140 kDa (Fig. 1E). Next, DIR-labeled MC-ELNs were prepared to determine their biodistribution using NEWTON imaging. We observed predominant DIR-MC-ELNs fluorescent signals in the liver and spleen 24 h after tail vein administration. The DIR-MC-ELNs fluorescent signal was higher in the heart than that of DIR, indicating MC-ELNs could reach the heart (Fig. 1F, Figure S1). Last, we performed proteomic, non-targeted metabolomic, and lipidomic assays to analyze the composition of MC-ELNs. We identified 2 389 proteins in the MC-ELNs group, 88.74% of which had molecular weights around 10 ~ 80 kDa (Fig. 1G). The top five ranked proteins are localized to the cytoplasm (33.86%), secreted (17.41%), nucleus (17.33%), chloroplast (11.8%), and mitochondrion (7.03%) (Fig. 1H, Table S1). MC-ELNs contained metabolomic agents like fatty acyls (32.69%) and steroids and its derivatives (14.42%) (Fig. 1I, Table S2), and lipid agents like TG (26.86%) and Cer (24.18%) (Fig. 1J,Table S3). Overall, MC-ELNs exhibited features identical to mammalian-derived EVs.

#### MC-ELNs improve cardiac function and myocardial structure in DOX cardiotoxicity animal models

We first explored the in vivo therapeutic efficiency of MC-ELNs in DOX cardiotoxicity mice model. Acute DOX cardiotoxicity mice model was established by a single dose injection of DOX (15 mg/kg) in C57BL/6J mice. We intravenously injected MC-ELNs (800–1200 μg/kg) or PBS into mice every two days (once before and three times after DOX injection) and sacrificed the mice the next day after the last injection (Fig. 2A). Cardiac injury markers such as cardiac troponin T (cTnT) and creatine kinase-MB (CK-MB) were lower in MC-ELNs-treated mice compared with only DOX-treated mice (Fig. 2B). At the histological level, MC-ELNs alleviated cardiac atrophy (Fig. 2C) and increased cardiomyocyte size (Fig. 2D) compared to DOX-treated mice. Because the two doses of MC-ELNs treatment displayed similar protective effects in DOX cardiotoxicity, we employed the lower dose to confirm their therapeutic activity in rat model. We intravenously injected MC-ELNs (800 μg/kg) or PBS into rat every two days (once before and twice

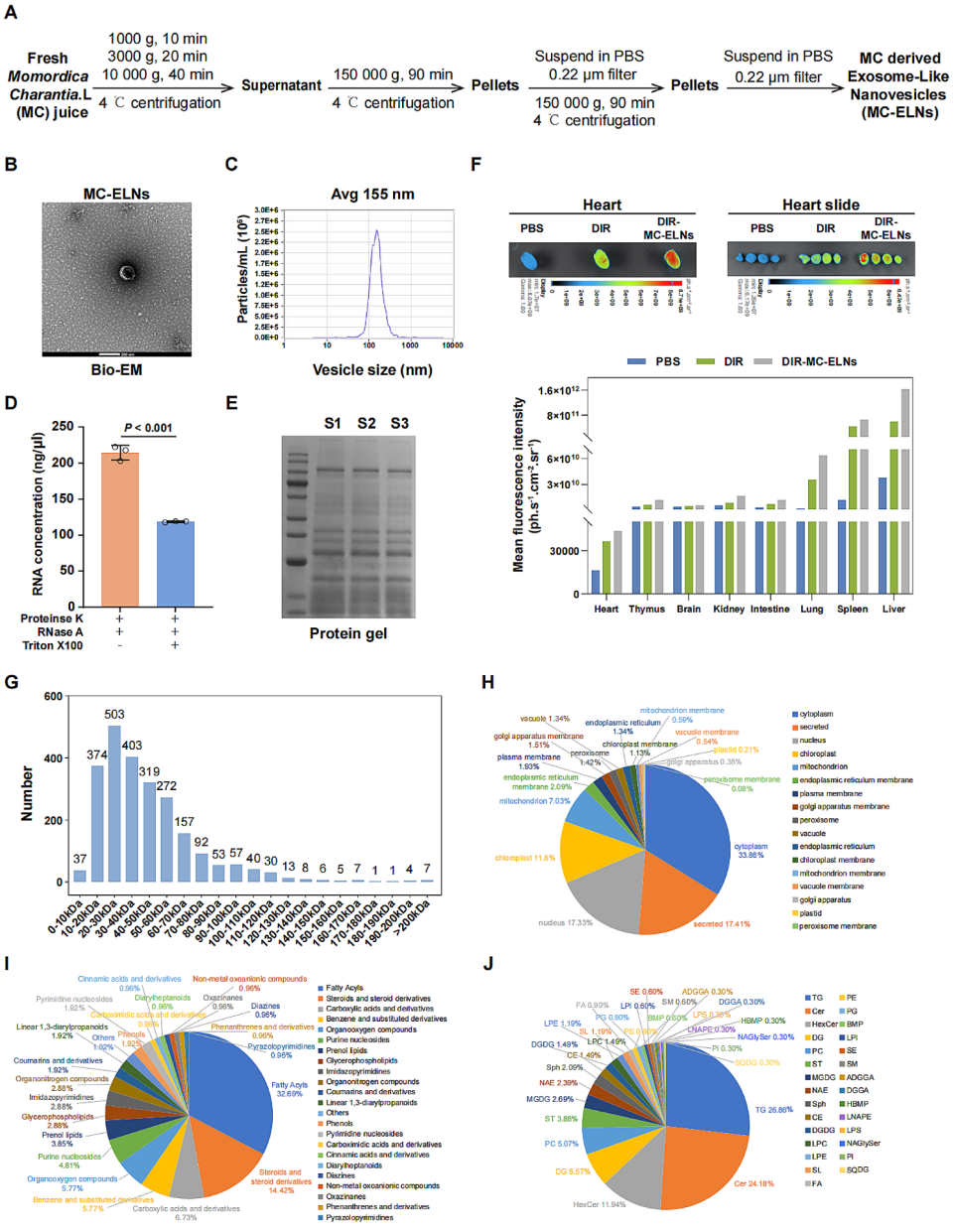


**Fig. 1** Isolation and identification of MC-ELNs. (**A**) Overall isolation procedures of MC-ELNs from fresh *Momordica Charantia* L. (MC) juice. (**B**) Biological electron microscope (Bio-EM) image on the morphology of MC-ELNs. Scale bar: 200 nm. (**C**) NTA analysis showed that the average size of MC-ELNs was around 155 nm. (**D**) MC-ELNs were incubated with RNase A in the presence or absence of Triton X100 to assess RNA integrity protected by the lipid bilayer membrane of extracellular vesicles. (**E**) MC-ELNs proteins were extracted and separated using SDS-PAGE, and then stained by Coomassie brilliant blue dye. (**F**) In vivo distribution of MC-ELNs. After 24 h of intravenously injection of PBS, DIR, DIR-MC-ELNs to C57BL/6J mice, ex vivo images and quantitative fluorescent intensity of various tissues, including liver, spleen, lung, intestine, kidney, brain, thymus, heart, and sectioned heart tissue were acquired with an Vilber Bio Imaging system. Representative images of heart and sectioned heart tissue (upper). Quantitative data on the in vivo fluorescent signals of various tissues (down). Compositional analysis of MC-ELNs was performed, including the molecular weights distribution of identified proteins (**G**) and analysis on the proteomic (**H**), metabolomic (**I**), lipidomic (**J**) components in the MC-ELNs. All data are presented as mean ± SD ($n = 3$ experiments per group for **D**, **E**, **G-J**; $n = 1$ experiment per group for **F**). Comparisons between two groups were performed using two-tailed unpaired student's t-test

after DOX injection) and evaluated the cardiac function the next day after the last injection (Fig. 2E). MC-ELNs-treated mice hearts showed enhanced functional benefits with improved ejection fraction, fraction shortening, heart rate, left ventricular dimensions at end-systole, and end-systolic volume (Fig. 2F). H&E (Fig. 2G) and WGA (Fig. 2H, I) staining also demonstrated that hearts treated with MC-ELNs had diminished cardiac and cardiomyocyte atrophy. In addition, MC-ELNs-treated rat exhibited reduced serum cTnT and CK-MB levels (Fig. 2J). Taken together, these results indicated that MC-ELNs protected against DOX cardiotoxicity in both mice and rats.

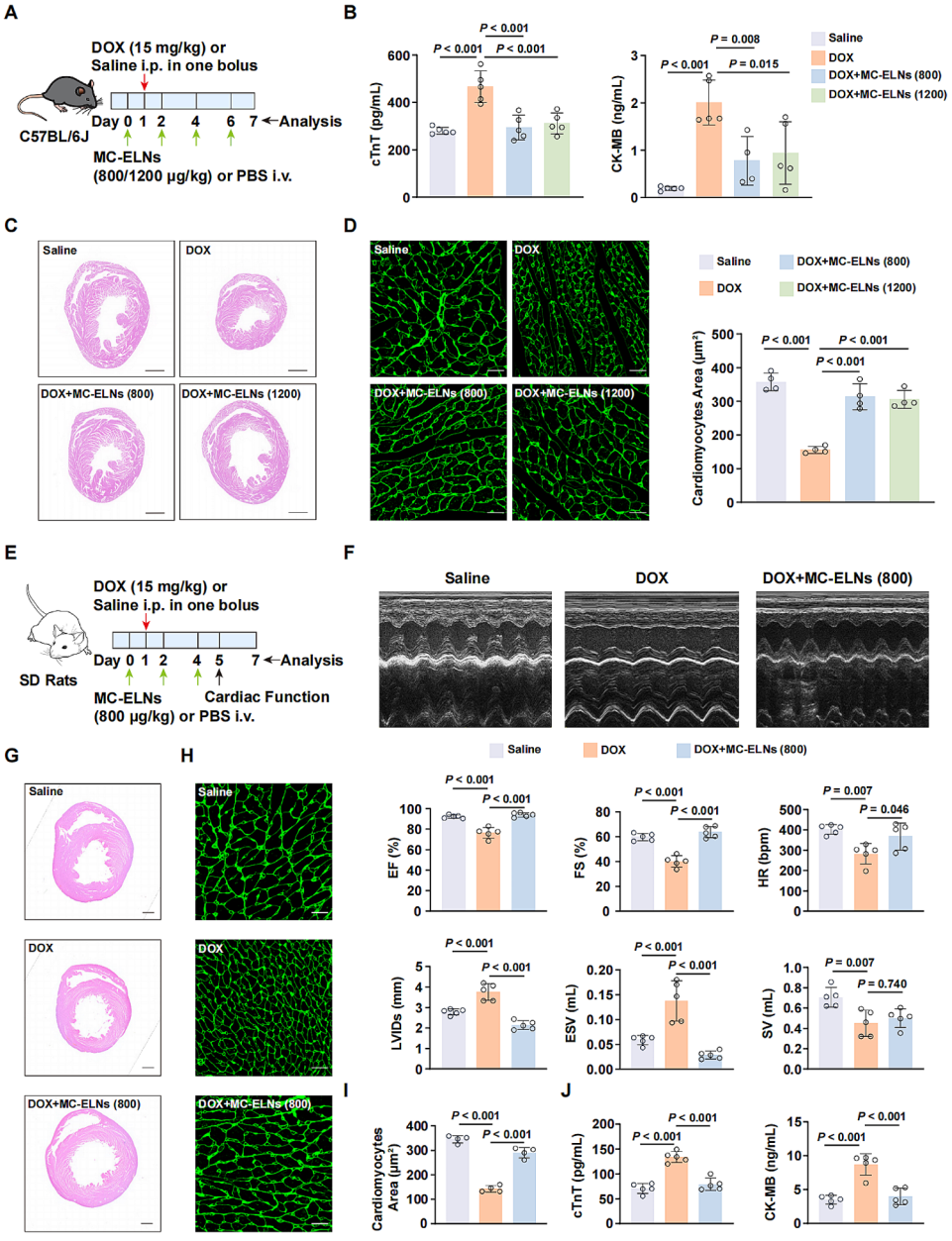


**Fig. 2** MC-ELNs prevent DOX cardiotoxicity in mice and rat models. (**A**) Experiment design timeline. Male 8–12 weeks old C57BL/6J mice were treated with vehicle or MC-ELNs (800–1200 μg/kg, every two days) intravenously one day before a single dose of saline or doxorubicin (DOX, 15 mg/kg) and continued for three times. (**B**) Serum cardiac injury biomarkers levels, including cTnT and CK-MB in each group of mice. (**C**) Representative H&E staining images in mouse hearts after indicated treatment. Scale bar: 1 mm. (**D**) Representative images of wheat germ agglutinin (WGA) staining in mouse hearts and quantitative data of cardiomyocytes area in each group. Scale bar: 20 μm. (**E**) Experiment design timeline. Male SD rats weighed 220–250 g were treated with vehicle or MC-ELNs (800 μg/kg, every two days) intravenously one day before a single dose of saline or DOX (15 mg/kg) and continued for twice. (**F**) Representative M-mode echocardiographic images of rats and quantitative data on the parameters, including ejection fraction (EF), fractional shortening (FS), heart rate (HR), left ventricular dimensions at end-systole (LVIDs), end-systolic volume (ESV), and stroke volume (SV) at 5-day point. (**G**) Representative H&E staining images in rat hearts after indicated treatment. Scale bar: 2 mm. (**H**, **I**) Representative images of WGA staining in rat hearts and quantitative data of cardiomyocytes area in each group. Scale bar: 20 μm. (**J**) Serum cardiac injury biomarkers levels, including cTnT and CK-MB in each group of rats. All data are presented as mean ± SD ($n = 4$ to 5 animals per group). Comparisons among more than two groups were performed by ordinary one-way analysis of variance (ANOVA) followed by the Tukey's multiple comparisons test

**MC-ELNs promote survival of DOX-treated cardiomyocyte without comprising DOX efficency in breast cancer cell line**

We first determined the optimal dose of DOX (1 μM) to induce injury in H9c2 cells using MTT assay (Fig. 3A). We next assessed that MC-ELNs enhanced the cell viability of DOX-treated H9c2 cells dose-dependently (Fig. 3B). MTT and LDH activity assay indicated that the MC-ELNs did not generate toxicity to H9c2 cells up to 25 μg/mL (Fig. 3C, D). Notably, we also investigated whether the MC-ELNs would influence the anti-tumor efficiency of DOX in vitro. DOX markedly provoked cell death in breast cancer cell line MCF-7 in comparison with the PBS control, and the cell viability was not enhanced by MC-ELNs with the same doses added to the cardiomyocytes (Figure S2A). The apoptosis markers Cleaved caspase3 and Cleaved PARP levels were slightly higher in the DOX-treated MCF-7 cells when supplemented with 10 μg/mL of MC-ELNs (Figure S2B, C). Moreover, MC-ELNs did not promote MCF-7 cells proliferation as the cell viability and levels of proliferation markers PCNA,

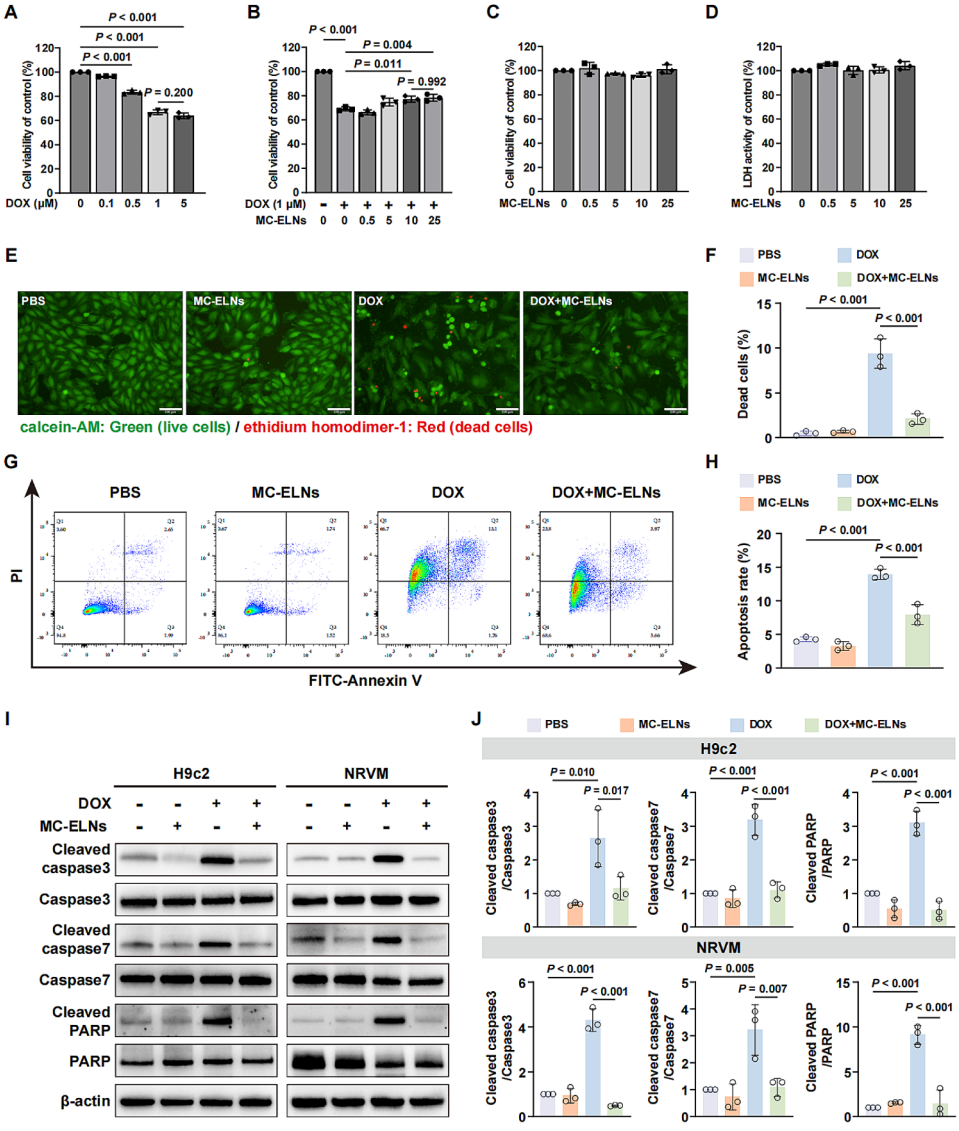


**Fig. 3** MC-ELNs suppress DOX-induced cell death in cardiomyocytes. (**A**) MTT assay identified the optimal concentration of doxorubicin (DOX, 1 μM) for inducing H9c2 cells death. (**B**) MTT assay revealed the best doses of MC-ELNs (10 μg/mL) for inhibiting DOX-induced H9c2 cells loss. MC-ELNs did not impair the cell viability (**C**) and generate toxicity (**D**) to H9c2 cells. (**E**) Representative calcein AM and ethidium homodimer-1 staining images for cell viability of H9c2 cells treated with 1 μM DOX in the absence or presence of 10 μg/mL MC-ELNs. The green fluorescence indicated live cells and red fluorescence indicated dead cells, respectively. Scale bar: 100 μm. (**F**) Histogram displays quantitative data for **E**. (**G**) Representative flow cytometry images for cell apoptosis of H9c2 cells treated with 1 μM DOX in the absence or presence of 10 μg/mL MC-ELNs. (**H**) Histogram displays quantitative data for **G**. (**I**, **J**) Western blot analysis on the protein levels of apoptosis markers in H9c2 cells or neonatal rat ventricular myocyte cells (NRVM) treated with 1 μM DOX in the absence or presence of 10 μg/mL MC-ELNs. All data are presented as mean ± SD ($n = 3$ experiments per group). Comparisons among more than two groups were performed by ordinary one-way analysis of variance (ANOVA) followed by the Tukey's multiple comparisons test

Cyclin B1, and Cyclin E1 were indistinguishable when cultured with different doses of MC-ELNs for 24 h and 48 h (Figure S2D-F). We employed 10 μg/mL of MC-ELNs for further experiments because the survival rate between the addition of 10 and 25 μg/mL of MC-ELNs was not significantly different. The calcein AM and ethidium homodimer-1 staining another assay to evaluate cell viability revealed a robust increase in H9c2 cells death after DOX treatment, which was markedly decreased to 2-fold in the presence of MC-ELNs (Fig. 3E, F). Flow cytometry apoptosis analysis showed that MC-ELNs reduced the apoptosis rate of DOX-treated H9c2 cells (Fig. 3G, H). In addition, the elevated protein levels of apoptosis markers, including Cleaved caspase3, Cleaved caspase7, and Cleaved PARP in DOX-treated H9c2 cells and neonatal rat ventricular myocytes (NRVM) were declined by the addition of MC-ELNs (Fig. 3I, J). Overall, the above data implied that MC-ELNs enhanced cardiomyocytes cell survival against DOX and did not interfere with DOX efficacy in killing tumor cells.

#### MC-ELNs attenuate oxidative stress, maintain mitochondrial structure, enhance cell proliferation in DOX-treated cardiomyocytes

Given that DOX can generate excessive radicals and MC extract has antioxidant activity, the ability of MC-ELNs to scavenge reactive oxygen species in cells (ROS) and mitochondria (MitoSOX) was investigated (Fig. 4A). In H9c2 cells, DOX increased the ROS and MitoSOX fluorescence intensity, and the MC-ELNs led to a 50% reduction of ROS and MitoSOX levels (Fig. 4B). Because mitochondria dysfunction is one of the major pathways triggering DOX cardiotoxicity, we assessed the integrity of mitochondrial using MitoTracker staining. Different from the highly interconnected mitochondria in PBS-treated cells, mitochondria in the DOX-treated H9c2 cells presented as round and smaller fragments (Fig. 4A). The quantitative analysis of mitochondrial morphology (Fig. 4C) showed that mean branch length and mitochondrial footprint sizes were markedly declined, numbers of individuals and networks were increased with a reduced mean individual and network sizes in DOX-treated H9c2 cells compared with PBS-treated cells. As expected, DOX-induced mitochondrial structural damage was protected by MC-ELNs. In addition to the oxidative stress on DNA double-strand, DOX disrupts topoisomerase II β activity, resulting in DNA damage and cell cycle arrest in cardiomyocytes. As shown by western blot analysis (Fig. 4D, E), MC-ELNs recovered the expressions of DNA injury marker γ-H2A.X and cell cycle-related proteins, including Cyclin D1 and Cyclin E1 in H9c2 cells after DOX treatment. By the immunofluorescence staining of cell proliferation marker Ki-67, we identified a significantly decreased percentage of Ki-67 positive H9c2 cells in the presence of DOX, which were dramatically enhanced by MC-ELNs (Fig. 4F, G). From these data, MC-ELNs improved redox equilibrium, restored mitochondrial function, promoted cell proliferation in the DOX-treated H9c2 cells.

#### MC-ELNs mitigate DOX-induced cardiomyocytes apoptosis not by the regulation of autophagy

Autophagy is another critical pathway involved in DOX cardiotoxicity, which always overlaps and cross-talks with apoptosis signaling, determining the cell fate of cardiomyocytes. We observed time-dependent decreased levels of LC3B II, a hallmark of autophagosome formation, and the p62 in DOX (1 μM, 24 h)-treated H9c2 cells (Figure S3A). Autophagy activity is quantitated by autophagic flux [20]. The 4th edition of autophagy guidelines raises a caution that the ratio of LC3B II/I at a single timepoint indicates autophagic "carrier flux" rather than the actual autophagic cargo/substrate flux [21]. The autophagic flux should be evaluated by comparing the levels of LC3B II with treatment alone and with lysosomal inhibition or interfering with autophagosome-lysosome fusion (e.g., CQ). Compared with the PBS-treated H9c2 cells, the levels of LC3B II were declined by DOX treatment alone. The CQ (50 μM, 4 h) treatment promoted LC3B II accumulation in both PBS- and DOX-treated H9c2 cells. However, the levels of LC3B II were lower in the DOX + CQ group than in the CQ group (Figure S3B). We also monitored autophagic flux in H9c2 cells at 0, 8, 12, and 24 h after DOX treatment using the mcherry-EGFP-LC3B reporter assay (Figure S3C, D). DOX treatment gradually increased autophagosomes ($GFP^+/mcherry^+$) but decreased autolysosomes ($GFP^-/mcherry^+$) in H9c2 cells. Thus, DOX causes a partially blocked autophagic flux at late stages in H9c2 cells. Next, we determined whether the MC-ELNs could regulate the autophagy process. The mcherry-EGFP-LC3B reporter assay showed that DOX-induced accumulation of autophagosomes were significantly reduced by MC-ELNs treatment (Figure S4A, B). In addition, it showed higher LC3B II levels with MC-ELNs treatment in DOX-treated H9c2 cells (Figure S4C), and the levels of LC3B II were higher in the DOX + MC-ELNs + CQ group than in the DOX + CQ group (Figure S4F), implicating that MC-ELNs attenuated DOX-induced inhibition of autophagy in H9c2 cells. To further verify the role of autophagy in the cardioprotective action by MC-ELNs, we additionally treated H9c2 cells with autophagy activator Rapa (100 nM, 24 h) or autophagy inhibitor CQ (5 μM, 24 h). Rapa further decreased apoptosis markers levels in DOX-treated H9c2 cells in the presence of MC-ELNs or not (Figure S4E). However, the MC-ELNs reduced apoptosis markers levels were not increased by CQ treatment (Figure S4F). Thus, MC-ELNs mitigate DOX-induced H9c2 cells apoptosis not by the regulation of autophagy.

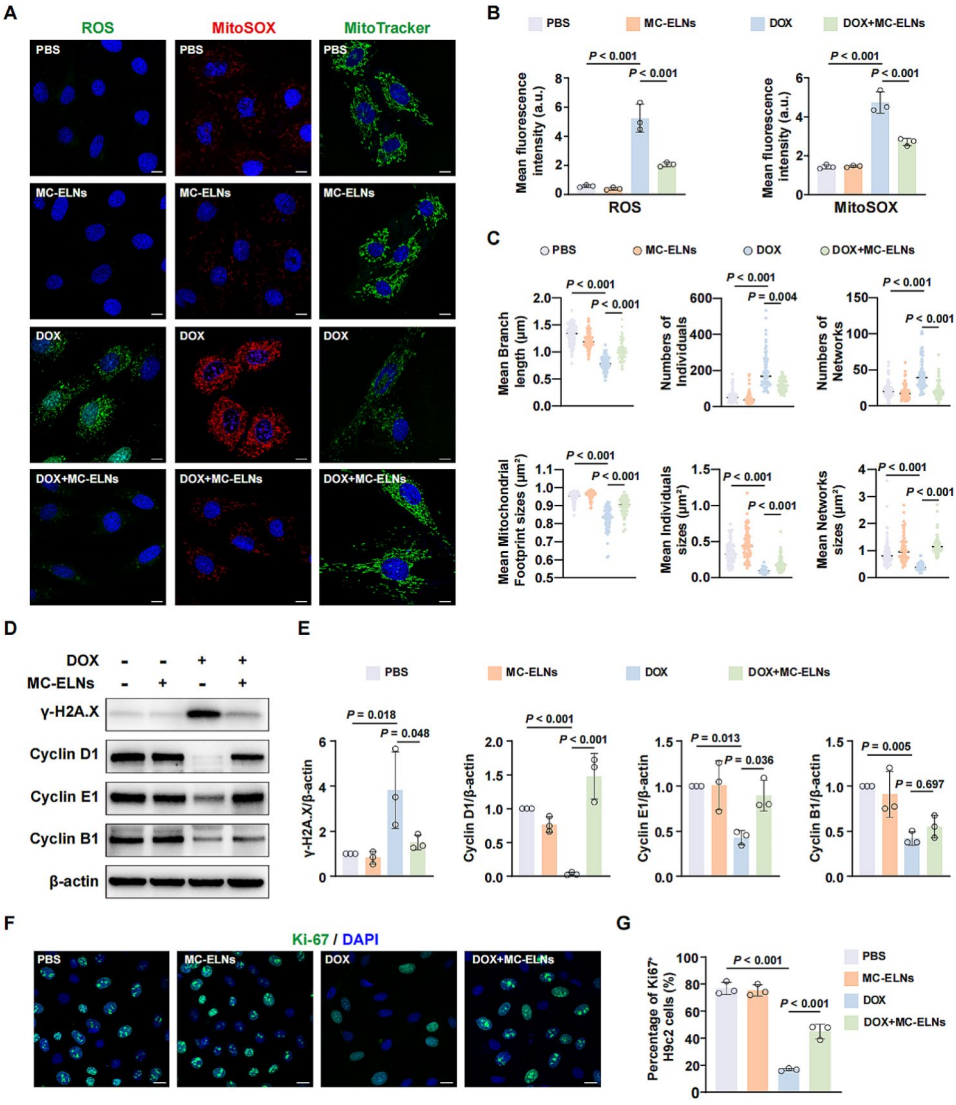


**Fig. 4** MC-ELNs maintain redox equilibrium and relieve cell cycle arrest in DOX-treated cardiomyocytes. (**A**) Representative images on the intracellular (ROS) and mitochondrial reactive oxygen species (MitoSOX), mitochondrial morphology (MitoTracker) of H9c2 cells treated with 1 μM doxorubicin (DOX) in the absence or presence of 10 μg/mL MC-ELNs. Scale bar: 20 μm. (**B**) Quantitative data on the levels of ROS and MitoSOX in each group. (**C**) Mitochondrial analysis was compared in 75 cells of 3 replicates. Each dot represented the quantitative data of mitochondria in a single cell. (**D**, **E**) Western blot analysis and quantitative data on the levels of DNA damage and cell cycle markers in H9c2 cells treated with 1 μM DOX in the absence or presence of 10 μg/mL MC-ELNs. (**F**, **G**) Representative images and quantitative data on the Ki-67 positive H9c2 cells treated with 1 μM DOX in the absence or presence of 10 μg/mL MC-ELNs. Scale bar: 20 μm. All data are presented as mean ± SD ($n = 3$ experiments per group). Comparisons among more than two groups were performed by ordinary one-way analysis of variance (ANOVA) followed by the Tukey's multiple comparisons test (**B**, **E**, **G**), Brown-Forsythe and Welch ANOVA tests followed by the Tamhane T2 multiple comparisons test (branch length in **C**), or Kruskal-Wallis test followed by Dunn's multiple comparisons test (individuals, networks, individuals sizes, network sizes footprint sizes in **C**)

### MC-ELNs stabilize p62 expression in DOX-treated cardiomyocytes

Upon autophagy inhibition, the decreases in LC3B II was often accompanied by increased p62 levels [22]. However, our findings showed a marked decrease in the protein level of p62 in DOX-treated H9c2 cells and NRVM in contrast to the PBS-treated cells, which was further restored by MC-ELNs (Fig. 5A, B). Furthermore, the CQ treatment increased p62 level in PBS-treated H9c2 cells but even decreased p62 levels in DOX-treated H9c2 cells (Figure S4D, F). Notably, DOX significantly increased the mRNA level of p62 in H9c2 cells, and this increase was slightly reduced in the presence of MC-ELNs (Fig. 5C). Thus, we reasoned that DOX-induced loss of p62 was associated with regulation of proteasomal, not the autophagy. When we added lactacystin (LACTA) to inhibit proteasome activity, the protein level of p62 was increased compared to H9c2 cells treated with DOX alone, implying the DOX-induced p62 proteasome degradation (Fig. 5D). In addition, incubation with protein

synthesis inhibitor cycloheximide (CHX) revealed that MC-ELNs markedly elongated the half-life of p62 protein, indicating the enhanced p62 protein stability by MC-ELNs (Fig. 5E). The mechanism of MC-ELNs improving p62 protein stability was investigated next. Concordant with the alteration of p62 protein level, MC-ELNs generated a marked reduction in ubiquitination of p62 in H9c2 cells treated with DOX (Fig. 5F). Among which, compared with the DOX-treated H9c2 cells, the ubiquitination of p62 with K48-Ub and K63-Ub declined in the presence of MC-ELNs, and the reduced binding with K48-Ub was more than that of K63-Ub (Fig. 5F). Then, we analyzed the type of E3 ubiquitin ligase that regulated p62 ubiquitination (Fig. 5G, H, I). To our regret, the expressions of three well-established E3 ubiquitin ligase of p62 including Parkin, TRIM21, and TRAF6 were inconsistent with its changes of p62 protein levels, suggesting a novel E3 ubiquitin ligase regulating p62 degradation in this context. Collectively, our results showed that MC-ELNs prevented p62 from undergoing ubiquitination degradation in cardiomyocytes exposed to DOX.

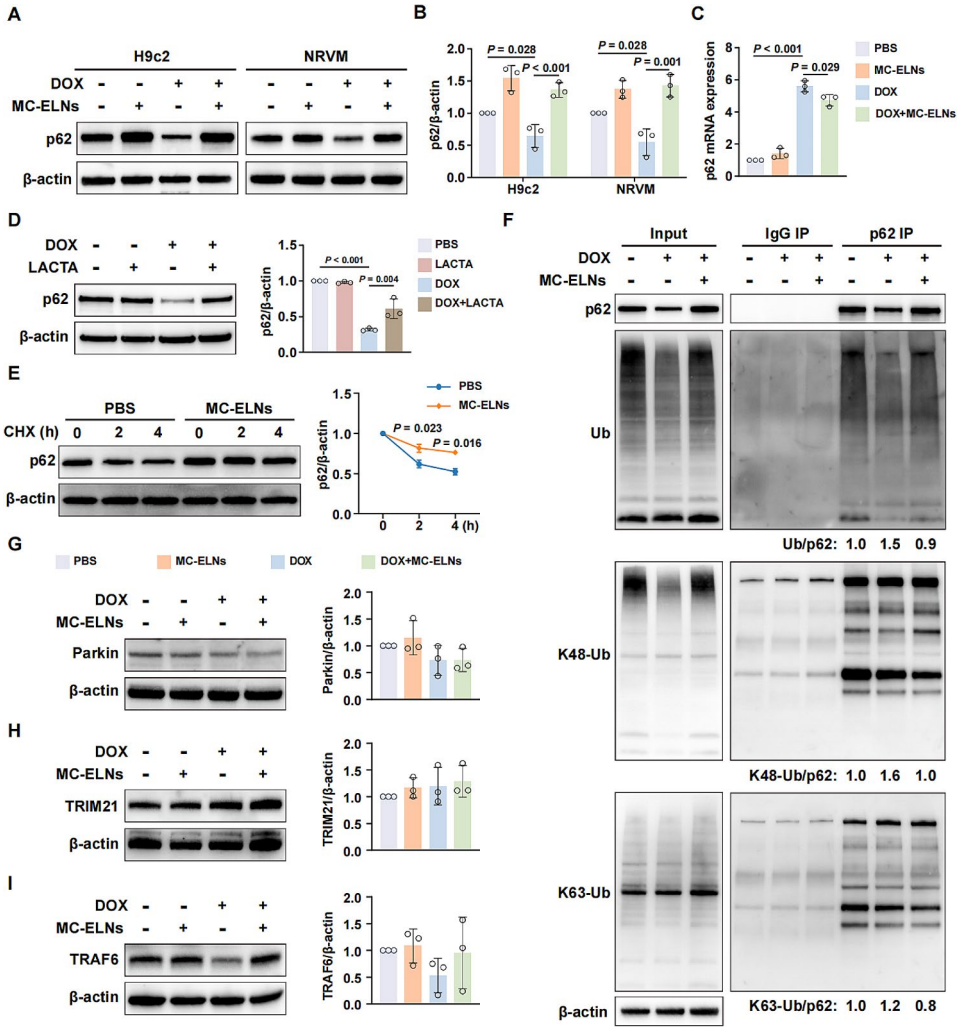


**Fig. 5** MC-ELNs prevent p62 from DOX-induced ubiquitination degradation in cardiomyocytes. H9c2 cells were pre-treated with 10 μg/mL MC-ELNs for 6 h, and then cultured with or without 1 μM doxorubicin (DOX) for another 24 h. Western blot images (**A**) and quantitative analysis (**B**) on the p62 protein levels. (**C**) The p62 mRNA levels in H9c2 cells treated with 1 μM DOX in the absence or presence of 10 μg/mL MC-ELNs. (**D**) H9c2 cells were treated with PBS or 1 μM DOX in the presence or absence of 2 μM Lactacystin (LACTA) for 24 h. (**E**) H9c2 cells were incubated in the absence or presence of MC-ELNs (10 μg/mL) in combination with the protein synthesis inhibitor cycloheximide (CHX, 10 μg/mL) for 2–4 h. Western blot analysis of the expressions of p62. (**F**) Immunoprecipitation assay (IP) and western blot analysis of cell lysate derived from PBS- or DOX-treated H9c2 cells in the absence or presence of 10 μg/mL of MC-ELNs (DOX, DOX + MC-ELNs). IP was performed with an antibody against p62. The blot was probed with antibodies against p62, Ub, K48-Ub, and K63-Ub. β-actin was employed as a loading control. Western blot analysis on the identified E3 ligase enzyme bound with p62 including Parkin (**G**), TRIM21 (**H**), and TRAF6 (**I**) in H9c2 cells treated with 1 μM DOX in the absence or presence of 10 μg/mL MC-ELNs. All data are presented as mean ± SD ($n = 3$ experiments per group for **A**-**E**, **G**-**I**; $n = 1$ experiment per group for **F**). Comparisons among more than two groups were performed by ordinary one-way analysis of variance (ANOVA) followed by the Tukey's multiple comparisons test

### MC-ELNs mitigate the DOX-induced cardiomyocytes apoptosis via p62/Keap1/Nrf2 pathway

It is known that p62-Keap1 interaction promotes Nrf2 activation and its downstream signaling cascade [23]. We detected markedly reduced Keap1 levels in DOX-treated H9c2 cells and NRVM, which were slightly increased by the MC-ELNs treatment (Fig. 6A). Co-IP analysis (Fig. 6B) and immunofluorescence staining (Fig. 6C) revealed the binding of Keap1 with p62. Thus, we further evaluated whether Nrf2 and its downstream signaling HO-1 were activated. Immunofluorescence images displayed declined Nrf2 levels in DOX-treated H9c2 cells and MC-ELNs promoted the nuclear translocation of Nrf2 (Fig. 6D). Consistently, the Nrf2 and HO-1 levels were decreased in DOX-treated H9c2 cells and NRVM, which were further improved in the presence of MC-ELNs (Fig. 6E, F). We further checked the levels of Nrf2 downstream gene NQO1 and other antioxidant enzyme such as Catalase, SOD2, and GPX4 after DOX or MC-ELNs treatment. We found that the levels of NQO1 (Figure S5A) and Catalase (Figure S5B) were decreased by DOX treatment, which were restored by further MC-ELNs treatment. However, though DOX treatment increased the levels of SOD2, but MC-ELNs treatment did not decrease SOD2 levels compared to DOX alone (Figure S5C). The levels of GPX4 were not affected by the DOX or MC-ELNs treatment (Figure S5D). Moreover, transfection with Nrf2 siRNA significantly decreased the elevated protein levels of Nrf2 and HO-1, whereas enhanced the expression of Cleaved caspase3 and Cleaved PARP in DOX-treated H9c2 cells after MC-ELNs treatment (Fig. 6G). Because p62 competes with Nrf2 for Keap1 binding, we investigated the therapeutic effects of MC-ELNs by adding the K67, a p62-Keap1 interaction inhibitor. The disruption of p62-Keap1 binding led to decreased Nrf2 and increased Keap1 levels in DOX-treated H9c2 cells in the presence of MC-ELNs (Fig. 6H). In line with this result, the cytoprotective effects of MC-ELNs were inhibited by K67 treatment in DOX-treated H9c2 cells (Fig. 6H).

## Discussion

Emerging evidence has indicated that P-ELNs displayed innate therapeutic properties. P-ELNs from ginger were reported to ameliorate colitis via delivering miR-167a [24], inhibit NLRP3 inflammasome activation [25], exert anti-obesity activity via miR-375 [26], activate Nrf2 pathway to treat dermatitis [27] and alcohol-induced liver injury [28]. These observations suggested that P-ELNs from one kind of plant may have various biological effects, reflecting the diversity in their constituents and targets. We previously reported that MC-ELNs exerted cardioprotective effects against ionizing radiation [13], warranting explorations on the role of MC-ELNs in the cardiotoxicity caused by other anti-cancer therapies, for instance, the DOX. In this study, we investigated the features of MC-ELNs in-depth, whether they prevented DOX cardiotoxicity, and the underlying mechanisms. Our data showed that MC-ELNs were enriched in RNA, proteins, lipids, and metabolites. The intravenous administration of MC-ELNs recovered cardiac function and myocardial structure in acute DOX cardiotoxicity mice and rat models. In addition, MC-ELNs enhanced cell survival, counteracted oxidative stress, and preserved mitochondrial structure in DOX-treated cardiomyocytes without comprising the anti-cancer effect of DOX in MCF-7 breast cancer cell line. Furthermore, we specifically observed a p62 ubiquitination and proteasomal degradation in cardiomyocytes exposed to DOX, which were inhibited by MC-ELNs treatment. Subsequently, upregulated p62 bound with Keap1, which promoted the nuclear translocation of oxidative stress transcription factor Nrf2, reducing cardiomyocytes apoptosis.

Oxidative stress is established as the primary pathological contributor to DOX cardiotoxicity [29]. In addition, DOX readily accumulates in mitochondria, leading to mitochondrial ROS production and mitochondria dysfunction [1]. Here, we found that MC-ELNs reduced the intracellular and mitochondrial ROS and protected mitochondrial integrity. The disruption of topoisomerase enzyme by DOX confers to its anti-cancer potency and toxicity to cardiac. DOX inhibited topoisomerase II β function in cardiomyocytes, which caused DNA damage and cell cycle arrest [30]. MC-ELNs decreased the level of DNA damage and attenuated cell cycle arrest in the H9c2 cells after DOX treatment. To further investigate the mechanism of MC-ELNs in attenuating DOX cardiotoxicity, we evaluated the changes of cell survival pathway in cardiomyocytes, such as autophagy and proteasomal degradation.

The role of autophagy in DOX cardiotoxicity is still ambiguous. Multiple studies have reported the overstimulation of autophagy by DOX and autophagy inhibitors prevented DOX cardiotoxicity in cellular models [31, 32]. The accumulated autophagosomes were thought to eliminate intracellular organelles excessively, causing cell death [33]. Conversely, others observed inhibition of autophagy [34] or Parkin-mediated mitophagy [35] in DOX-treated cardiac cells. In this case, the injured cellular organelles could not be cleared promptly, and activation of autophagy before DOX therapy appears beneficial in protecting cardiac function. These mixed reports may be attributed to the difference in model or cell lines, DOX concentration, and incubation time. It has identified that autophagy was inhibited in H9c2 cells exposed to DOX (1 μM) for 48 h [36], or starved H9c2 cells exposed to DOX (1 μM) for 24 h [37]. Our data indicated an inhibition of autophagy in H9c2 cells treated with DOX (1 μM) for

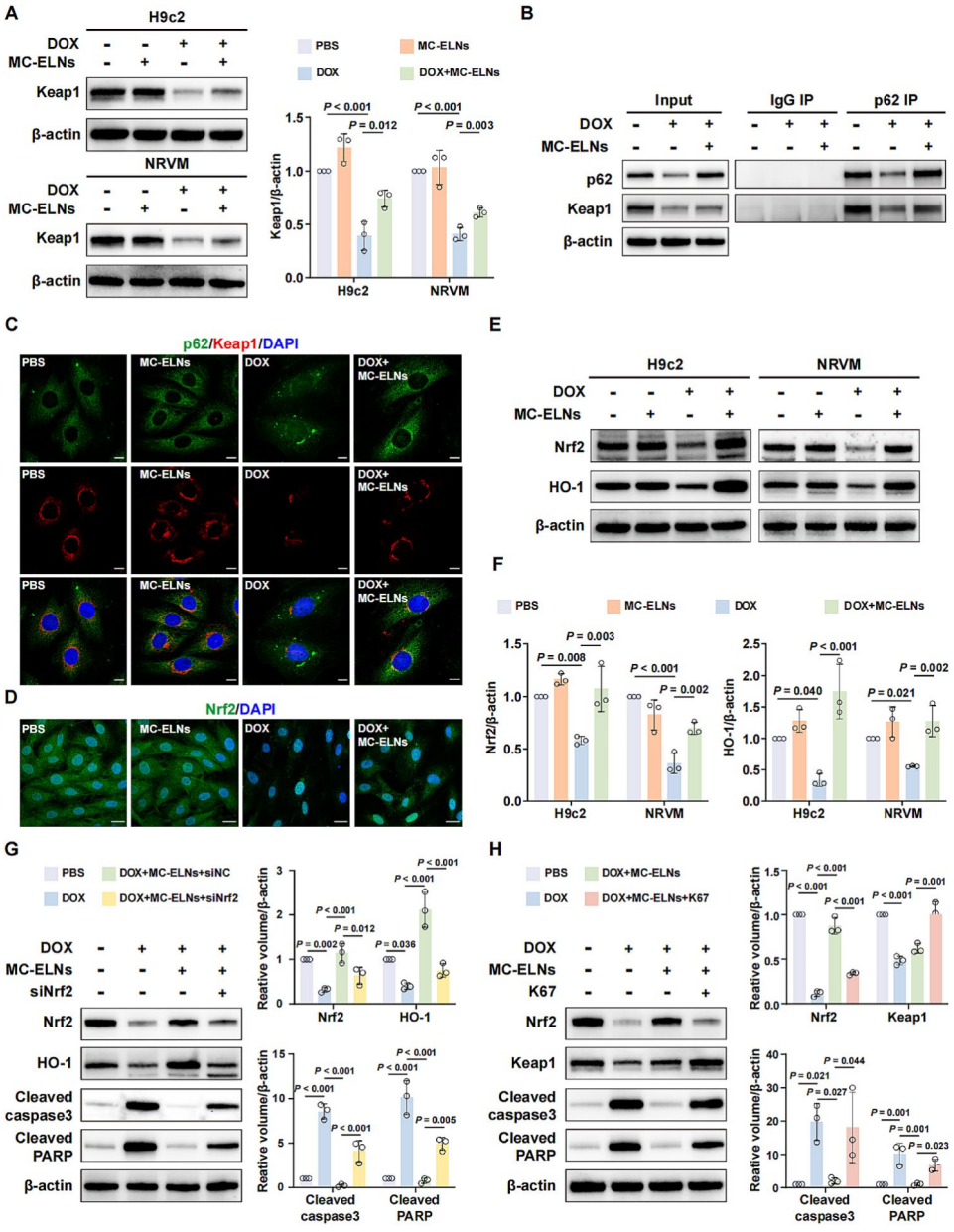


**Fig. 6** MC-ELNs reduce DOX-induced cardiomyocytes apoptosis via regulating p62/Keap1/Nrf2 pathway. (**A**) H9c2 cells or NRVM were pre-treated with 10 μg/mL MC-ELNs for 6 h, and then cultured with or without 1 μM doxorubicin (DOX) for another 24 h. Western blot analysis of Keap1 levels. (**B**) Immunoprecipitation assay (IP) and western blot analysis of cell lysate derived from PBS- or DOX-treated H9c2 cells in the absence or presence of 10 μg/mL of MC-ELNs (DOX, DOX + MC-ELNs). IP was performed with an antibody against p62. The blot was probed with antibodies against p62 and Keap1. β-actin was employed as a loading control. (**C**) Confocal microscopy analysis of the co-localization of Keap1 and p62. Scale bar: 10 μm. (**D**) Representative fluorescence images of Nrf2 expressions in H9c2 cells with indicated treatment. Scale bar: 20 μm. (**E**, **F**) Western blot analysis of Nrf2 and HO-1 in H9c2 cells treated with 1 μM DOX in the absence or presence of 10 μg/mL MC-ELNs. (**G**) After treatment and 2-day incubation with Nrf2 siRNA, H9c2 cells were treated with 1 μM DOX in the absence or presence of 10 μg/mL MC-ELNs. Western blot analysis of Nrf2, HO-1, Cleaved capsase3, and Cleaved PARP. (**H**) H9c2 cells were treated with 1 μM DOX in the absence or presence of 10 μg/mL MC-ELNs or K67 (100 μM, Keap1-p62 interaction inhibitor) as indicated. Western blot analysis of Nrf2, Keap1, Cleaved capsase3, and Cleaved PARP. All data are presented as mean ± SD ($n = 3$ experiments per group for **A**, **B**, **E**-**H**; $n = 1$ experiments per group for **C**, **D**). Comparisons among more than two groups were performed by ordinary one-way analysis of variance (ANOVA) followed by the Tukey's multiple comparisons test

24 h, among which the partially blocked autophagy flux was further enhanced by MC-ELNs. However, adding autophagy inhibitor CQ to deplete the autophagy activation effect by MC-ELNs did not abolish its protective effects. Thus, we speculated that the cardioprotective effect of MC-ELNs may result from other mechanism.

Interestingly, we noticed a decreased protein level of p62, a ubiquitin-binding protein, in DOX-treated H9c2

cells and NRVM, which was supposed to be increased upon autophagic flux inhibition [38]. However, there is not always a definite correlation between increases in LC3B II and decreases in p62 when autophagy inhibition occurs [39]. Hence, p62 is not a proper marker in assessing autophagy flux. In fact, we assessed elevated mRNA level of p62 in H9c2 cells after DOX treatment, suggesting a post-translational modification of p62. Inhibition of proteasome activity further confirmed a ubiquitin proteasome degradation of p62 in DOX-treated H9c2 cells. In addition, our result demonstrated that MC-ELNs notably decreased the ubiquitination of p62 with K48-Ub in DOX-treated H9c2 cells, in which the K48-Ub generally targets substrates for proteasomal degradation [40]. p62 can interact with ubiquitinated substrates via its ubiquitin-associated domain, and then recruits the ubiquitinated aggregates cargoes to proteasome via its N-terminal Phox-BEM1 domain [41] or to autophagy machinery via its LC3-interacting region [42]. Therefore, p62 may play an important role in the cross talk between the ubiquitin-proteasome system and autophagic lysosomal pathway [39]. Wang et al. showed that systemic proteasome inhibition induced myocardial autophagy via upregulating the calcineurin-TFEB-p62 pathway [43]. Herein, it is highly likely that the improved autophagy flux by MC-ELNs was consequence of its effects on increasing p62 protein level. Imaoka et al. identified that Parkin bound with p62 via the PB1 domain, leading to p62 proteasomal degradation in hepatocellular carcinoma cells under hypoxia [44]. Zong et al. demonstrated that TRIM21 ubiquitylates p62 which prevent its bound with Keap1 and subsequent Nrf2 antioxidant pathway [45], and the loss of TRIM21 mitigates DOX cardiotoxicity [46]. The interaction of zing finger ZZ domain with RIP1 and TRAF6-binding domain with TRAF6 regulates the NF-κB pathway [47]. In this study, the above mentioned E3 ubiquitin ligase such as Parkin, TRIM21, and TRAF6 protein levels was inconsistent with altered p62 protein levels with indicated treatment, respectively. Further studies are needed to identify the specific E3 ubiquitin ligases and associated mechanisms promoting proteasomal degradation of p62 in DOX cardiotoxicity.

We also examined the potential cardioprotective mechanism of p62 in DOX-treated cardiomyocytes. p62 is a highly conserved protein with multi-domain and multifunctional adaptor involved in the regulation of inflammation and cancer [48]. Being a chaperone for selective autophagy, p62 is identified a major player in cardiometabolic disease including atherosclerosis, nonalcoholic fatty liver disease, obesity, and type 2 diabetes [49]. p62 can regulate PINK1/Parkin-mediated mitophagy and mitochondrial quality control. However, it showed no significant differences on the Parkin levels between the DOX and DOX plus MC-ELNs group, suggesting that PINK1/Parkin-mediated mitophagy not involved in the cardioprotective action of MC-ELNs. The other known function of p62 is its rising affinity for Keap1 that responsible for degrading Nrf2, resulting in the activation of stress responsive transcription factor Nrf2 [50, 51]. The activation of p62/Keap1/Nrf2 pathway have shown protective effects in ischemic [52] or cisplatin [53]-induced cardiac injury. Indeed, we confirmed a combination of p62 with Keap1 using Co-IP analysis and confocal imaging. As the protein levels of p62 and Keap1 were markedly deceased, the enhanced binding of p62 with Keap1 may contribute to maintain the cell survival in DOX-treated H9c2 cells. After the supplement of MC-ELNs in DOX-treated H9c2 cells, although the protein level of p62 was increased to normal levels, the protein level of Keap1 was still lower than that of normal cells, which resulted in insufficient binding of p62 with Keap1 compared with DOX group. MC-ELNs promoted Nrf2 nuclear translocation and enhanced the Nrf2 and HO-1 levels in DOX-treated H9c2 cells and NRVM. Moreover, the knockdown of Nrf2 and disruption of p62-Keap1 interaction markedly abolished the cardioprotective effects of MC-ELNs. Thus, the therapeutic beneficials of MC-ELNs depended on the increasing p62 protein stability. Taking past studies into consideration, we propose that DOX mediates p62 ubiquitination degradation and MC-ELNs stabilize p62 expressions, rendering more p62 binding with Keap1 to promote Nrf2 nuclear translocation and downstream gene HO-1 activation (Fig. 7).

This study has several limitations. First, MC-ELNs comprised diverse biomolecules such as lipids, proteins, and RNAs, and we did not pinpoint the specific active components crucial for their therapeutic efficacy. Growing evidence stated that EVs' function is more likely attributed to the synergetic effects of their constituents [54]. Brucea jaavanica-derived exosome-like nanovesicles delivered 10 functional miRNAs for cancer therapy [55]. Our group also identified 81 miRNAs enriched in MC-ELNs, and the top 3 are miR6135, miR5813, and miR408, respectively [11]. Nevertheless, further exploration of the active contents conferring MC-ELNs' cardioprotective action, is imperative for translating research findings into clinically applicable interventions. Second, we only preliminarily examined the in vivo cardioprotective effects of intravenous administrated MC-ELNs in acute DOX cardiotoxicity animal models with a relatively small sample size. The fluorescence intensity observed in the heart is notably lower compared to other tissues, raising concerns regarding the long-term cardioprotective efficacy of MC-ELNs. In addition, it is doubted that the intravenous administration of MC-ELNs may introduce the possibility of unforeseen side effects due to the diverse nature of the substances they contain. The in

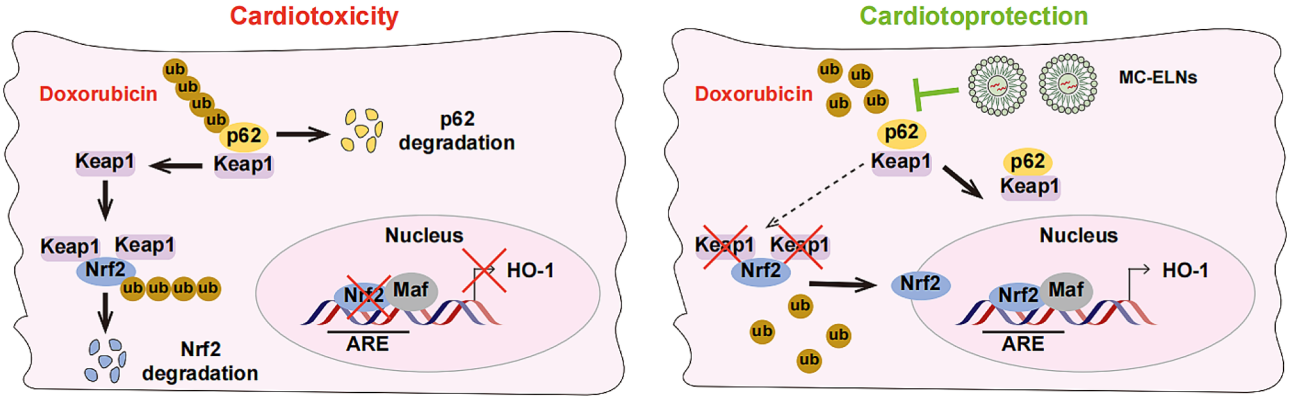


**Fig. 7** Schematic illustration of the mechanisms underlying the cardioprotective effects of MC-ELNs via stabilizing p62 expression. Doxorubicin led to p62 ubiquitination proteasomal degradation in cardiomyocytes. MC-ELNs stabilized p62 expression to promote its competition with Nrf2 for Keap1 binding, promoting nuclear translocation of Nrf2 and its downstream gene HO-1 activation. MC-ELNs, *Momordica charantia* L.-derived exosome-like nanovesicles

vitro MTT and LDH assay demonstrated the nontoxicity of MC-ELNs to H9c2 cells and our group showed that the intravenous administration of MC-ELNs did not induce tissue injury in the rat (unpublished data). Thus, we will further confirm the in vivo therapeutic efficacy of MC-ELNs in both acute and chronic DOX cardiotoxicity animal models using different delivery venues (e.g., oral administration) with a proper sample size. The FDA approved dexrazoxane for preventing DOX cardiotoxicity will be involved as a positive control/standard drug to compare the cardioprotective effect of MC-ELNs [56]. Last, we mainly first focused on the investigation of the cardioprotective potential of MC-ELNs. Regarding the future clinical application of MC-ELNs, we just simply proved that MC-ELNs did not interfere with DOX efficacy in killing MCF-7 cancer cells and did not promote MCF-7 cells proliferation in vitro. We previously confirmed MC-ELNs could inhibit the proliferation, migration, and invasion of glioma cell [11]. Indeed, cancer cells exhibit unique mitochondrial bioenergetics and biosynthetic states compared to normal cells. It would be of interest to explore the in vivo biological effect and associated mechanisms of MC-ELNs in both cardiac and cancer cells by establishing a tumor animal model with DOX treatment.

## Conclusions

In conclusion, we demonstrated that MC-ELNs proved beneficial in mitigating DOX cardiotoxicity via stabilizing p62 protein level. MC-ELNs may be a perfect cyto-protective agent because it attenuates chemotherapy-induced injuries in normal tissue cells without diminishing the efficacy of chemotherapy in killing the cancer cells. Further studies are warranted to elucidate the molecular mechanism involved in MC-ELNs-induced stabilizing p62 protein level and its role in DOX cardiotoxicity.

### Abbreviations

| | |
|---|---|
| Bio-EM | Biological electron microscopy |
| Cer | Ceramide |
| CHX | Cycloheximide |
| CK-MB | Creatine Kinase-MB |
| CQ | Chloroquine |
| cTnT | Cardiac Troponin T |
| DOX | Doxorubicin |
| ESV | End-Systolic Volume |
| EVs | Extracellular Vesicles |
| FS | Fraction Shortening |
| HR | Heart Rate |
| LACTA | Lactacystin |
| LDH | Lactate dehydrogenase |
| LVEF | Left Ventricular Ejection Fraction |
| LVIDs | Left Ventricular Dimensions at end-systole |
| MC-ELNs | *Momordica charantia* L.-Derived Exosome-Like Nanovesicles |
| MTT | 3-(4,5-Dimethylthiazol-2-yl)-2,5-diphenyltetrazolium bromide |
| NRVM | Neonatal Rat Ventricular Myocyte Cells |
| NTA | Nanoparticle Tracking Analysis |
| P-ELNs | Plant-derived Exosome-Like Nanovesicles |
| Rapa | Rapamycin |
| SV | Stroke Volume |
| TG | Triacylglycerol |
| WGA | Wheat Germ Agglutinin |

## Supplementary Information

The online version contains supplementary material available at https://doi.org/10.1186/s12951-024-02705-z.

Supplementary Material 1

### Acknowledgements

The experiments in this article were partially completed in Public Experimental Research Center of Xuzhou Medical University, and thanks the teachers Dr. Fu-Xing Dong for their support and help during the experiments.

### Author contributions

C.Y. and C.Y. contributed equally to this work. C.Y. and C.Y. performed experiments, analyzed the data, drafted and revised the manuscript and figures. S.J.B., X.R.L., Y.L., K.X.W., Y.H.Z., L.W., and Y.C.W. performed experiments and analyzed the data. T.S.L. provided intellectual discussions on experimental designs. S.H.Q and L.L conceived and supervised the project, edited and

revised the manuscript. All authors have given approval to the final version of the manuscript.

**Funding**
This work was supported by the National Natural Science Foundation of China (grant no. 82270360), the Natural Science Foundation of Jiangsu Province (grant no. BK20231183), the Scientific Research Project of Jiangsu Provincial Healthy Commission (grant no. ZDB2020024), the Postgraduate Research & Practice Innovation Program of Jiangsu Province (grant no. KYCX23_2939), the National Demonstration Center for Experiment Basic Medical Science Education (Xuzhou Medical University, grant no. 202010313013Z), the Project of Science and Technology Department of Jiangxi Province (grant no. 20204BCJ23018), the Young Science and Technology Innovation Team (grant no. TD202005) and the Leadership program (grant no. JBGS202203) of Xuzhou Medical University.

**Data availability**
No datasets were generated or analysed during the current study.

## Declarations

**Competing interests**
The authors declare no competing interests.

Received: 27 February 2024 / Accepted: 5 July 2024
Published online: 02 August 2024

**References**

1. Wu L, Wang L, Du Y, Zhang Y, Ren J. Mitochondrial quality control mechanisms as therapeutic targets in doxorubicin-induced cardiotoxicity. Trends Pharmacol Sci. 2023;44:34–49.
2. Sawicki KT, Sala V, Prever L, Hirsch E, Ardehali H, Ghigo A. Preventing and treating Anthracycline Cardiotoxicity: New insights. Annu Rev Pharmacol Toxicol. 2021;61:309–32.
3. Abushouk AI, Ismail A, Salem AMA, Afifi AM, Abdel-Daim MM. Cardioprotective mechanisms of phytochemicals against doxorubicin-induced cardiotoxicity. Biomed Pharmacother. 2017;90:935–46.
4. Rawat PS, Jaiswal A, Khurana A, Bhatti JS, Navik U. Doxorubicin-induced cardiotoxicity: an update on the molecular mechanism and novel therapeutic strategies for effective management. Biomed Pharmacother. 2021;139:111708.
5. Han C, Yang J, Sun J, Qin G. Extracellular vesicles in cardiovascular disease: Biological functions and therapeutic implications. Pharmacol Ther. 2022;233:108025.
6. Lian MQ, Chng WH, Liang J, Yeo HQ, Lee CK, Belaid M, Tollemeto M, Wacker MG, Czarny B, Pastorin G. Plant-derived extracellular vesicles: recent advancements and current challenges on their use for biomedical applications. J Extracell Vesicles. 2022;11:e12283.
7. Cong M, Tan S, Li S, Gao L, Huang L, Zhang HG, Qiao H. Technology insight: plant-derived vesicles-how far from the clinical biotherapeutics and therapeutic drug carriers? Adv Drug Deliv Rev. 2022;182:114108.
8. Hwang JH, Park YS, Kim HS, Kim DH, Lee SH, Lee CH, Lee SH, Kim JE, Lee S, Kim HM, et al. Yam-derived exosome-like nanovesicles stimulate osteoblast formation and prevent osteoporosis in mice. J Control Release. 2023;355:184–98.
9. Wang S, Li Z, Yang G, Ho CT, Li S. Momordica charantia: a popular health-promoting vegetable with multifunctionality. Food Funct. 2017;8:1749–62.
10. Yang M, Luo Q, Chen X, Chen F. Bitter melon derived extracellular vesicles enhance the therapeutic effects and reduce the drug resistance of 5-fluorouracil on oral squamous cell carcinoma. J Nanobiotechnol. 2021;19:259.
11. Wang B, Guo X-J, Cai H, Zhu Y-H, Huang L-Y, Wang W, Luo L, Qi S-H. Momordica charantia-derived extracellular vesicles-like nanovesicles inhibited glioma proliferation, migration, and invasion by regulating the PI3K/AKT signaling pathway. J Funct Foods. 2022;90:104968.
12. Cai H, Huang LY, Hong R, Song JX, Guo XJ, Zhou W, Hu ZL, Wang W, Wang YL, Shen JG, Qi SH. Momordica charantia Exosome-Like nanoparticles exert neuroprotective effects against ischemic brain Injury via Inhibiting Matrix Metalloproteinase 9 and activating the AKT/GSK3beta signaling pathway. Front Pharmacol. 2022;13:908830.
13. Cui WW, Ye C, Wang KX, Yang X, Zhu PY, Hu K, Lan T, Huang LY, Wang W, Gu B, et al. Momordica. Charantia-derived extracellular vesicles-like Nanovesicles Protect Cardiomyocytes against Radiation Injury via attenuating DNA damage and Mitochondria Dysfunction. Front Cardiovasc Med. 2022;9:864188.
14. Ibrahim AG, Cheng K, Marban E. Exosomes as critical agents of cardiac regeneration triggered by cell therapy. Stem Cell Rep. 2014;2:606–19.
15. Lou D, Wang Y, Yang Q, Hu L, Zhu Q. Ultrafiltration combing with phospholipid affinity-based isolation for metabolomic profiling of urinary extracellular vesicles. J Chromatogr A. 2021;1640:461942.
16. Sun C, Liang H, Zhao Y, Li S, Li X, Yuan X, Cheng G, Zhang Y, Liu M, Guan Y, et al. Jingfang Granules improve glucose metabolism disturbance and inflammation in mice with urticaria by up-regulating LKB1/AMPK/SIRT1 axis. J Ethnopharmacol. 2023;302:115913.
17. Aljobaily N, Viereckl MJ, Hydock DS, Aljobaily H, Wu TY, Busekrus R, Jones B, Alberson J, Han Y. Creatine alleviates Doxorubicin-Induced Liver damage by inhibiting liver fibrosis, inflammation, oxidative stress, and Cellular Senescence. Nutrients. 2020;13:nu13010041.
18. Vandergriff AC, Hensley MT, Cheng K. Isolation and cryopreservation of neonatal rat cardiomyocytes. J Vis Exp 2015:52726.
19. Yoshii SR, Mizushima N. Monitoring and measuring autophagy. Int J Mol Sci 2017, 18.
20. Ueno T, Komatsu M. Monitoring autophagy flux and activity: principles and applications. BioEssays. 2020;42:e2000122.
21. Klionsky DJ, Abdel-Aziz AK, Abdelfatah S, Abdellatif M, Abdoli A, Abel S, Abeliovich H, Abildgaard MH, Abudu YP, Acevedo-Arozena A et al. Guidelines for the use and interpretation of assays for monitoring autophagy (4th edition) (1). *Autophagy* 2021, 17:1-382.
22. Pugsley HR. Assessing Autophagic Flux by measuring LC3, p62, and LAMP1 co-localization using Multispectral Imaging Flow Cytometry. J Vis Exp 2017.
23. Jiang T, Harder B, de la Rojo M, Wong PK, Chapman E, Zhang DD. p62 links autophagy and Nrf2 signaling. Free Radic Biol Med. 2015;88:199–204.
24. Teng Y, Ren Y, Sayed M, Hu X, Lei C, Kumar A, Hutchins E, Mu J, Deng Z, Luo C, et al. Plant-derived exosomal MicroRNAs shape the gut microbiota. Cell Host Microbe. 2018;24:637–e652638.
25. Chen X, Zhou Y, Yu J. Exosome-like nanoparticles from Ginger rhizomes Inhibited NLRP3 inflammasome activation. Mol Pharm. 2019;16:2690–9.
26. Kumar A, Ren Y, Sundaram K, Mu J, Sriwastva MK, Dryden GW, Lei C, Zhang L, Yan J, Zhang X, et al. miR-375 prevents high-fat diet-induced insulin resistance and obesity by targeting the aryl hydrocarbon receptor and bacterial tryptophanase (tnaA) gene. Theranostics. 2021;11:4061–77.
27. Park G, Oh DS, Lee MG, Lee CE, Kim YU. 6-Shogaol, an active compound of ginger, alleviates allergic dermatitis-like skin lesions via cytokine inhibition by activating the Nrf2 pathway. Toxicol Appl Pharmacol. 2016;310:51–9.
28. Zhuang X, Deng ZB, Mu J, Zhang L, Yan J, Miller D, Feng W, McClain CJ, Zhang HG. Ginger-derived nanoparticles protect against alcohol-induced liver damage. J Extracell Vesicles. 2015;4:28713.
29. Kong CY, Guo Z, Song P, Zhang X, Yuan YP, Teng T, Yan L, Tang QZ. Underlying the mechanisms of Doxorubicin-Induced Acute Cardiotoxicity: oxidative stress and cell death. Int J Biol Sci. 2022;18:760–70.
30. Kuno A, Hosoda R, Tsukamoto M, Sato T, Sakuragi H, Ajima N, Saga Y, Tada K, Taniguchi Y, Iwahara N, Horio Y. SIRT1 in the cardiomyocyte counteracts doxorubicin-induced cardiotoxicity via regulating histone H2AX. Cardiovasc Res. 2023;118:3360–73.
31. Xu ZM, Li CB, Liu QL, Li P, Yang H. Ginsenoside Rg1 prevents Doxorubicin-Induced cardiotoxicity through the inhibition of Autophagy and endoplasmic reticulum stress in mice. Int J Mol Sci. 2018;19:ijms19113658.
32. Kobayashi S, Volden P, Timm D, Mao K, Xu X, Liang Q. Transcription factor GATA4 inhibits doxorubicin-induced autophagy and cardiomyocyte death. J Biol Chem. 2010;285:793–804.
33. Liu Y, Levine B. Autosis and autophagic cell death: the dark side of autophagy. Cell Death Differ. 2015;22:367–76.
34. Li DL, Wang ZV, Ding G, Tan W, Luo X, Criollo A, Xie M, Jiang N, May H, Kyrychenko V, et al. Doxorubicin blocks Cardiomyocyte Autophagic Flux by inhibiting lysosome acidification. Circulation. 2016;133:1668–87.
35. Hoshino A, Mita Y, Okawa Y, Ariyoshi M, Iwai-Kanai E, Ueyama T, Ikeda K, Ogata T, Matoba S. Cytosolic p53 inhibits parkin-mediated mitophagy and promotes mitochondrial dysfunction in the mouse heart. Nat Commun. 2013;4:2308.
36. Liu D, Zhao L. Spinacetin alleviates doxorubicin-induced cardiotoxicity by initiating protective autophagy through SIRT3/AMPK/mTOR pathways. Phytomedicine. 2022;101:154098.

37. Gu J, Fan YQ, Zhang HL, Pan JA, Yu JY, Zhang JF, Wang CQ. Resveratrol suppresses doxorubicin-induced cardiotoxicity by disrupting E2F1 mediated autophagy inhibition and apoptosis promotion. Biochem Pharmacol. 2018;150:202–13.
38. Chen D, Yu W, Zhong C, Hong Q, Huang G, Que D, Wang Y, Yang Y, Rui B, Zhuang Z, et al. Elabela ameliorates doxorubicin-induced cardiotoxicity by promoting autophagic flux through TFEB pathway. Pharmacol Res. 2022;178:106186.
39. Liu WJ, Ye L, Huang WF, Guo LJ, Xu ZG, Wu HL, Yang C, Liu HF. p62 links the autophagy pathway and the ubiqutin-proteasome system upon ubiquitinated protein degradation. Cell Mol Biol Lett. 2016;21:29.
40. Grice GL, Nathan JA. The recognition of ubiquitinated proteins by the proteasome. Cell Mol Life Sci. 2016;73:3497–506.
41. Wang C, Wang X. The interplay between autophagy and the ubiquitin-proteasome system in cardiac proteotoxicity. Biochim Biophys Acta. 2015;1852:188–94.
42. Turco E, Witt M, Abert C, Bock-Bierbaum T, Su MY, Trapannone R, Sztacho M, Danieli A, Shi X, Zaffagnini G, et al. FIP200 claw domain binding to p62 promotes autophagosome formation at Ubiquitin condensates. Mol Cell. 2019;74:330–e346311.
43. Pan B, Li J, Parajuli N, Tian Z, Wu P, Lewno MT, Zou J, Wang W, Bedford L, Mayer RJ, et al. The Calcineurin-TFEB-p62 pathway mediates the activation of Cardiac Macroautophagy by Proteasomal Malfunction. Circ Res. 2020;127:502–18.
44. Siswanto FM, Mitsuoka Y, Nakamura M, Oguro A, Imaoka S. Nrf2 and Parkin-Hsc70 regulate the expression and protein stability of p62/SQSTM1 under hypoxia. Sci Rep. 2022;12:21265.
45. Pan JA, Sun Y, Jiang YP, Bott AJ, Jaber N, Dou Z, Yang B, Chen JS, Catanzaro JM, Du C, et al. TRIM21 ubiquitylates SQSTM1/p62 and suppresses protein sequestration to regulate Redox Homeostasis. Mol Cell. 2016;61:720–33.
46. Hou K, Shen J, Yan J, Zhai C, Zhang J, Pan JA, Zhang Y, Jiang Y, Wang Y, Lin RZ, et al. Loss of TRIM21 alleviates cardiotoxicity by suppressing ferroptosis induced by the chemotherapeutic agent doxorubicin. EBioMedicine. 2021;69:103456.
47. Nakamura K, Kimple AJ, Siderovski DP, Johnson GL. PB1 domain interaction of p62/sequestosome 1 and MEKK3 regulates NF-kappaB activation. J Biol Chem. 2010;285:2077–89.
48. Hennig P, Fenini G, Di Filippo M, Karakaya T, Beer HD. The pathways underlying the multiple roles of p62 in inflammation and Cancer. Biomedicines 2021, 9.
49. Jeong SJ, Zhang X, Rodriguez-Velez A, Evans TD, Razani B. p62/SQSTM1 and selective autophagy in Cardiometabolic diseases. Antioxid Redox Signal. 2019;31:458–71.
50. Komatsu M, Kurokawa H, Waguri S, Taguchi K, Kobayashi A, Ichimura Y, Sou YS, Ueno I, Sakamoto A, Tong KI, et al. The selective autophagy substrate p62 activates the stress responsive transcription factor Nrf2 through inactivation of Keap1. Nat Cell Biol. 2010;12:213–23.
51. Ichimura Y, Waguri S, Sou YS, Kageyama S, Hasegawa J, Ishimura R, Saito T, Yang Y, Kouno T, Fukutomi T, et al. Phosphorylation of p62 activates the Keap1-Nrf2 pathway during selective autophagy. Mol Cell. 2013;51:618–31.
52. Zheng D, Liu Z, Zhou Y, Hou N, Yan W, Qin Y, Ye Q, Cheng X, Xiao Q, Bao Y, et al. Urolithin B, a gut microbiota metabolite, protects against myocardial ischemia/reperfusion injury via p62/Keap1/Nrf2 signaling pathway. Pharmacol Res. 2020;153:104655.
53. Jia Y, Guo H, Cheng X, Zhang Y, Si M, Shi J, Ma D. Hesperidin protects against cisplatin-induced cardiotoxicity in mice by regulating the p62-Keap1-Nrf2 pathway. Food Funct. 2022;13:4205–15.
54. Murphy DE, de Jong OG, Brouwer M, Wood MJ, Lavieu G, Schiffelers RM, Vader P. Extracellular vesicle-based therapeutics: natural versus engineered targeting and trafficking. Exp Mol Med. 2019;51:1–12.
55. Yan G, Xiao Q, Zhao J, Chen H, Xu Y, Tan M, Peng L. Brucea Javanica derived exosome-like nanovesicles deliver miRNAs for cancer therapy. J Control Release. 2024;367:425–40.
56. Fang X, Wang H, Han D, Xie E, Yang X, Wei J, Gu S, Gao F, Zhu N, Yin X, et al. Ferroptosis as a target for protection against cardiomyopathy. Proc Natl Acad Sci U S A. 2019;116:2672–80.


## Publisher's Note